Influence of chemical interaction at the lattice-mismatched *h*-BN/Rh(111) and *h*-BN/Pt(111) interfaces on the overlayer morphology

A. B. Preobrajenski,[1,*] A. S. Vinogradov,[2] May Ling Ng,[3] E. Ćavar,[4] R. Westerström,[4] A. Mikkelsen,[4] E. Lundgren,[4] and N. Mårtensson[1,3]

[1]*MAX-lab, Lund University, Box 118, 22100 Lund, Sweden*

[2]*V. A. Fock Institute of Physics, St.-Petersburg State University, 198504 St. Petersburg, Russia*

[3]*Department of Physics, Uppsala University, Box 530, 75121 Uppsala, Sweden*

[4]*Department of Synchrotron Radiation, Institute of Physics, Lund University, Box 118, 22100 Lund, Sweden*

(Received 16 December 2006; revised manuscript received 19 February 2007; published 12 June 2007)

The atomic and electronic structure of the lattice-mismatched *h*-BN/Pt(111) and *h*-BN/Rh(111) interfaces formed by pyrolitic reactions with vaporized borazine has been studied by low-energy electron diffraction, scanning tunneling microscopy, x-ray-absorption spectroscopy, and core-level and valence-band photoemission. It has been found that on Pt(111), *h*-BN forms a nearly flat monolayer, insignificantly corrugated across the supercell. On Rh(111), *h*-BN grows in form of a nanomesh, as originally observed by Corso *et al.* [Science **303**, 217 (2004)]. The structural difference between the *h*-BN/Pt(111) and *h*-BN/Rh(111) interfaces is associated with the strength of chemical interaction between *h*-BN and the substrate surface. A stronger orbital hybridization on Rh(111) results in a stronger attraction of the monolayer to the metal surface at favorable adsorption sites resulting in a highly corrugated structure (nanomesh). It has been shown that the electronic structure of the outer (elevated) and inner (attracted to the surface) nanomesh sites is very different as a result of different chemical bonding to the substrate (weak and strong, respectively).

DOI: 10.1103/PhysRevB.75.245412 PACS number(s): 68.37.Ef, 68.43.−h, 68.55.−a, 78.70.Dm

I. INTRODUCTION

Formation of hexagonal boron nitride (*h*-BN) on hot metal surfaces from molecular precursors has been studied for many years.[1–5] This interest has mainly been driven by the ability of boron nitride to form ultrathin well-ordered coatings, protecting the underlying substrate against oxidation. A classical example of *h*-BN/metal interfaces is a monolayer of *h*-BN formed on the lattice-matched Ni(111) substrate by thermal decomposition of molecular borazine ($B_3N_3H_6$).[2] Nowadays, the interest in *h*-BN films has been significantly augmented due to the ability of *h*-BN to form self-assembled nanostructures (nanomesh) on lattice-mismatched substrates, in particular, on Rh(111), as demonstrated by Corso *et al.*[6] This extraordinary ability makes *h*-BN a promising candidate for creating nanostructured templates for a variety of applications. However, the driving forces for the nanomesh formation remain unclear yet, although it is assumed that the mutual symmetry of the substrate and adsorbate and their lattice mismatch should be of considerable importance.[6]

On the other hand, the chemistry of the substrate may also be an important factor for the nanomesh formation. Recently, it has been shown that on transition-metal (TM) substrates, the interaction with *h*-BN is determined mainly by the orbital hybridization between the TM *d* states and the π states of *h*-BN.[7,8] Therefore, the strength of chemical bonding at the *h*-BN/TM interfaces must depend on the character of the substrate *d* states (energy, occupancy, and angular and radial distributions), varying from very weak to rather strong chemisorption. It seems plausible to assume that for lattice-mismatched systems with stronger interface bonding, the formation of the *h*-BN nanomesh is more probable than in the case of weaker interaction. Indeed, one can argue that a weakly bonded layer "levitates" above a lattice-mismatched substrate being relatively flat. In contrast, in the case of stronger interaction, the energy difference between favorable and unfavorable adsorption sites across the supercell of the coincidence lattice may become considerable leading to a strong corrugation of the *h*-BN sheet. In order to test this assumption, we compare in the present paper the interface bonding in two systems: *h*-BN/Rh(111) and *h*-BN/Pt(111). The in-plane lattice constants are 0.269 and 0.277 nm for Rh(111) and Pt(111), respectively, and 0.250 nm for bulk *h*-BN, resulting in mismatches of 7.6% and 10.8% for *h*-BN/Rh(111) and *h*-BN/Pt(111), respectively. Since the symmetry of the Rh(111) and Pt(111) surfaces is the same, it might be expected that the *h*-BN nanomesh can be formed on both substrates (with somewhat different period due to different mismatch), provided that the distinctions in the character of interface chemical bonding can be neglected. Whereas the formation of the *h*-BN nanomesh on Rh(111) is well documented by scanning tunneling microscopy (STM),[6] there exists no conclusive evidence either for or against the nanomesh formation on Pt(111). In the earlier study of *h*-BN on Pt(111), Paffet *et al.* observed some superperiodicity in low-energy electron diffraction (LEED), which was interpreted as being due to a hexagonal tenth-order coincidence lattice between *h*-BN and Pt(111).[1] However, the superperiodic LEED picture may result as well from a three-dimensional nanomesh. In the present paper, we show conclusively that the *h*-BN film formed on Pt(111) by thermal cracking of borazine is indeed a rather flat monolayer, and no nanomesh forms on this substrate.

Why does *h*-BN nanomesh form on Rh(111) but not on Pt(111) despite the same symmetry and a similar lattice mismatch? In order to answer this question, we report, analyze, and compare near-edge x-ray-absorption fine structure

(NEXAFS), as well as core-level and valence-band photoemission data, for both *h*-BN/Rh(111) and *h*-BN/Pt(111) interfaces. We show that the details of the electronic structure of the interfaces under study are very different, and we attribute this difference to the distinctly different orbital overlap of the Rh 4*d* and Pt 5*d* states with the *h*-BN π states. We associate the ability of *h*-BN to form nanomesh with a considerable strength of chemical interaction at the interface.

II. EXPERIMENT

The Rh(111) and Pt(111) substrates were cleaned by several cycles of Ar^+ sputtering ($U=2$ kV), heating in oxygen atmosphere [$p(O_2)=1\times10^{-7}$ mbar, $T=600-700$ °C], and annealing in UHV ($T=850$ °C for Pt and 950 °C for Rh). All temperatures were measured by a thermocouple directly attached to the crystals. The substrates were considered clean and well ordered if no contaminations could be detected by photoemission in the most surface-sensitive mode and a (1×1) LEED pattern with sharp spots could be observed. For the formation of *h*-BN, we used thermal cracking of vaporized borazine (purchased from BoroScience Canada), which was purified by several freeze-pump-thaw cycles. During borazine exposure the substrate temperature was maintained between 750 and 780 °C for both crystals. The borazine vapor exposure was typically above 100 L in order to ensure saturated *h*-BN coverage. Higher structural perfection of the resulting overlayers was observed for lower vapor pressure, which was typically set to 2×10^{-8} mbar.

The spectroscopic experiments were performed at the beamline D1011 at MAX II storage ring in MAX-lab (Lund, Sweden). The photon energy resolution was set to 50 meV at the B *K* edge (~190 eV) and to 150 meV at the N *K* edge (~400 eV). The kinetic-energy resolution of the SES-200 electron energy analyzer was set to 75 meV. The NEXAFS spectra were recorded in the partial electron yield mode (repulsive potential $U=-100$ V) by a multichannel plate detector and in the total electron yield mode by the sample current measurements. The spectral shapes were found to be nearly identical for these two methods in the case of thin *h*-BN overlayers. The base pressure during the measurements did not exceed 2×10^{-10} mbar. The NEXAFS spectra were normalized to the background curves recorded from clean substrates. The photon energies were calibrated using the difference in the kinetic energy of a photoelectron line recorded in the first- and second-order light.

Images were recorded using a commercial Omicron TS2 scanning tunneling microscope, operated at room temperature. The microscope is positioned inside an ultrahigh-vacuum system with a pressure better than 1×10^{-10} mbar. STM tips used in these experiments were chemically etched tungsten tips cleaned by Ar^+ sputtering. Samples for STM were prepared separately following the procedure described above.

III. RESULTS

A. LEED and STM

LEED patterns from the Rh(111) and Pt(111) substrates modified by pyrolitic growth of *h*-BN at the borazine exposure of 120 L are shown in Figs. 1(a) and 1(b), respectively. In both cases, principal substrate spots (indicated by crosses) are accompanied by a hexagonal network of diffraction spots due to the formation of an *h*-BN layer on the substrates. Analyzing the distances between substrate and adsorbate primary spots in the LEED patterns, we find *h*-BN-to-metal cell ratios of approximately 10:9 for Pt(111) and 13:12 for Rh(111), in accordance with previously reported values.[1,6] The LEED patterns do not allow distinguishing between a simple coincidence lattice and a three-dimensional overlayer superstructure with the same periodicity without a quantitative *I-V* LEED study, which in the present case is a formidable task due to the large number of atoms within the supercell. Therefore, it is hard to make any conclusion about the morphology of the *h*-BN overlayers on Rh(111) and Pt(111) from the LEED patterns only.

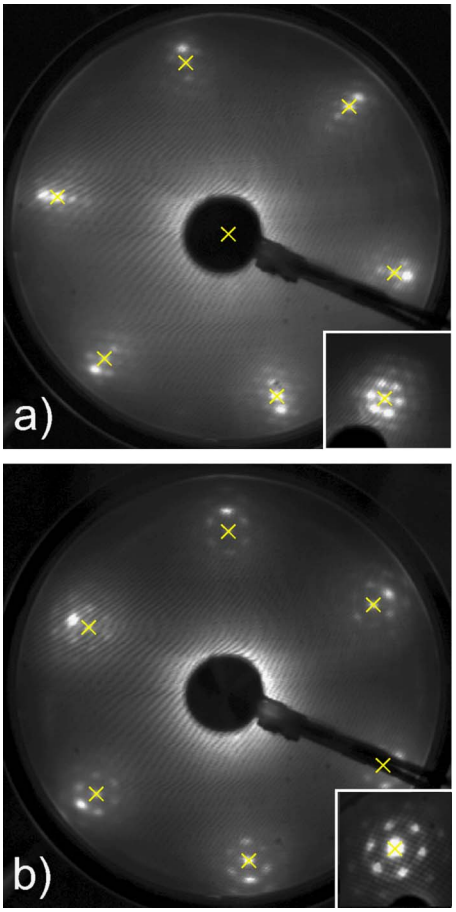

FIG. 1. (Color online) LEED patterns of the (a) *h*-BN/Rh(111) and (b) *h*-BN/Pt(111) interfaces recorded with the electron energy $E=60$ eV. Insets: images of the (0, 0) spots for the corresponding interfaces. Principal substrate spots are indicated by crosses.

The difference between the two systems can be seen in the STM images in Fig. 2. On Rh(111), *h*-BN forms a mesh with the periodicity of 3.2 ± 0.1 nm with the openings, whose structure could not be clearly resolved in our studies (upper image). According to the model proposed by Corso *et al.*, the atomically resolved structure comes from the corrugated top mesh of the double-layer *h*-BN nanomesh.[6] In another model presented by Laskowski *et al.*, the nanomesh structure is

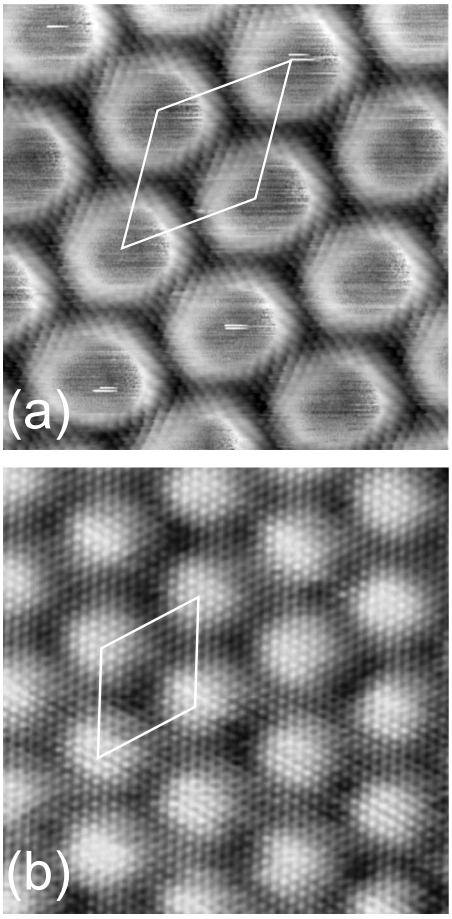

FIG. 2. Atomically resolved (10×10 nm^2) STM images of *h*-BN (a) on Rh(111) and (b) on Pt(111). The supercells are indicated. The tunneling parameters are $V=70$ mV, $I=3$ nA for (a) and $V=-10$ mV, $I=2$ nA for (b). Note the formation of a nanomesh on Rh(111) and a relatively flat monolayer on Pt(111).

proposed to result from a strongly corrugated single *h*-BN monolayer.[9] The STM images we obtained confirm a nanomesh structure of *h*-BN on Rh(111) but cannot distinguish between these two models. It is evident, however, that within each supercell (indicated by a rhombus in Fig. 2), there are sites which are hardly possible to image with atomic resolution simultaneously. This fact can be explained by a significant difference in the electronic structure of these sites resulting probably from different interactions with the substrate. We associate the atomically resolved sites in Fig. 2(a) with the weakly bonded (elevated) parts of the nanomesh and the unresolved areas—with the species directly contacting the substrate surface. Contrary to the case of *h*-BN/Rh(111), on Pt(111), each BN unit can be clearly imaged, accompanied by a moiré pattern [Fig. 2(b)], thus suggesting a single relatively flat *h*-BN monolayer. The moiré pattern results from the 10:9 coincidence lattice formed at the interface. It is also possible that the monolayer is slightly corrugated across the supercell. This corrugation may manifest itself in the STM images of Fig. 2(b) as a difference in intensity between fcc and hcp hollow sites of the supercell. On the other hand, it can also be a purely electronic effect (i.e., a part of the moiré pattern) due to the difference in the tunneling conditions for these two types of sites. In summary, the *h*-BN nanomesh can be formed on Rh(111) but not on Pt(111). In the following sections, we discuss why this happens.

B. X-ray absorption

Recently, we have shown that the element and symmetry selectivity of NEXAFS spectroscopy is very efficient in revealing the details of chemical interaction between *h*-BN and metal surfaces.[7,8] Besides, the polarization-dependent NEXAFS is ideally suited to characterize the structural perfection of the resulting *h*-BN overlayers. Figure 3 shows the B 1*s* [(a) and (b)] and N 1*s* [(c) and (d)] NEXAFS spectra measured from the complete *h*-BN overlayers formed on Pt(111) and Rh(111) as a function of angle between the polarization vector of incident light and the surface normal. As it can be expected for a layered system, the angle dependence is very pronounced, thus allowing us to easily distinguish between π states (features A'-A-A'') and σ states (all others) of *h*-BN. Evidently, the *h*-BN sheets are very flat and smooth on both substrates, because the π-related features disappear almost completely at normal incidence. The remaining at $\Theta=90°$ π-related intensity results probably from the substrate step edges and other defects, where the overlayer is forced to tilt or break.

Although the *h*-BN thickness is similar on both substrates [close to 1 ML (monolayer) due to the self-limiting nature of the pyrolitic reactions responsible for the layer growth], the spectra of *h*-BN look differently on Pt(111) and Rh(111). Indeed, in the B 1*s* NEXAFS spectra of *h*-BN on Rh(111), new shoulders A' and A'' develop on the low- and high-energy sides of peak A, respectively, and features B and C are less structured. In the N 1*s* NEXAFS spectra, similar spectral variations can be observed; moreover, a weak shoulder A' develops into a strong peak in going from *h*-BN/Pt(111) to *h*-BN/Rh(111). These differences clearly reflect considerable variations in chemical state of the interfaces as a consequence of essentially different orbital mixing (hybridization) of the substrate and adsorbate electronic states.

In order to estimate how strong is the chemical bonding at the interfaces under study, we should compare them with the previously studied cases of *h*-BN adsorption on Cu(111) and Ni(111).[8] These two substrates are both lattice matched to *h*-BN, have the same symmetry, but differ in the electronic structure due to the different radial distributions and occupations of the *d* orbitals. It has been shown that incomplete occupation of the *d* shell in the case of nickel results in a strong Ni 3*d*–*h*-BN π orbital mixing (strong covalent bonding), while at the *h*-BN/Cu(111) interface, the chemisorption is very weak due to the lack of such interfacial hybridization. In Fig. 4, the NEXAFS results for the *h*-BN/Pt(111) and *h*-BN/Rh(111) interfaces are presented together with the reference spectra for *h*-BN/Cu(111), *h*-BN/Ni(111), and bulk *h*-BN. The spectra are arranged such that from top to bottom the deviation from the bulk *h*-BN spectra increases, thus reflecting an increase in the interfacial orbital hybridiza-

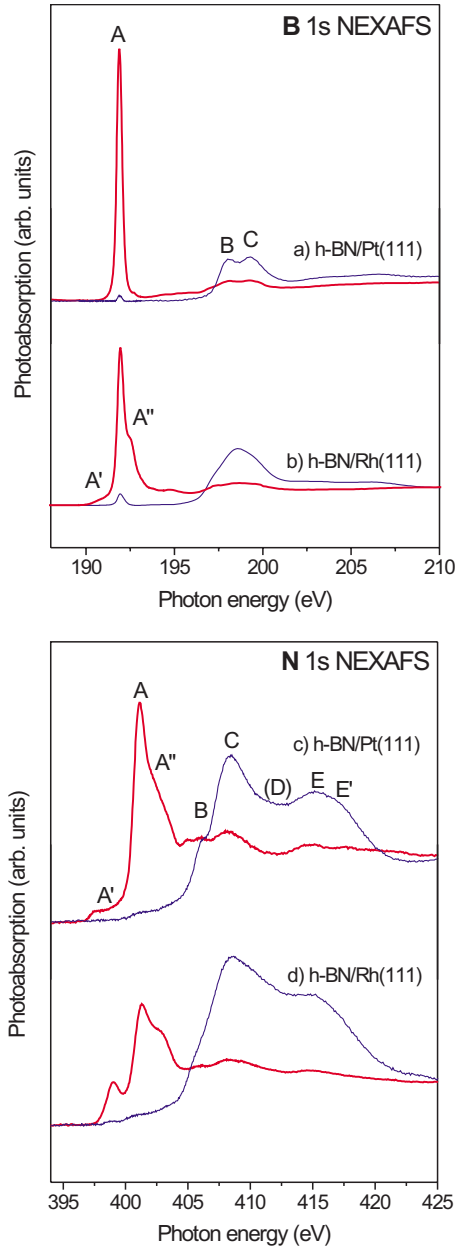

FIG. 3. (Color online) Angle-dependent B 1*s* and N 1*s* NEXAFS spectra of *h*-BN overlayers on [(a) and (c)] Pt(111) and on [(b) and (d)] Rh(111). Thicker (red) curves correspond to $\Theta = 20°$, and thinner (blue) curves correspond to $\Theta = 90°$ (Θ is the angle between surface normal and polarization vector of incident radiation).

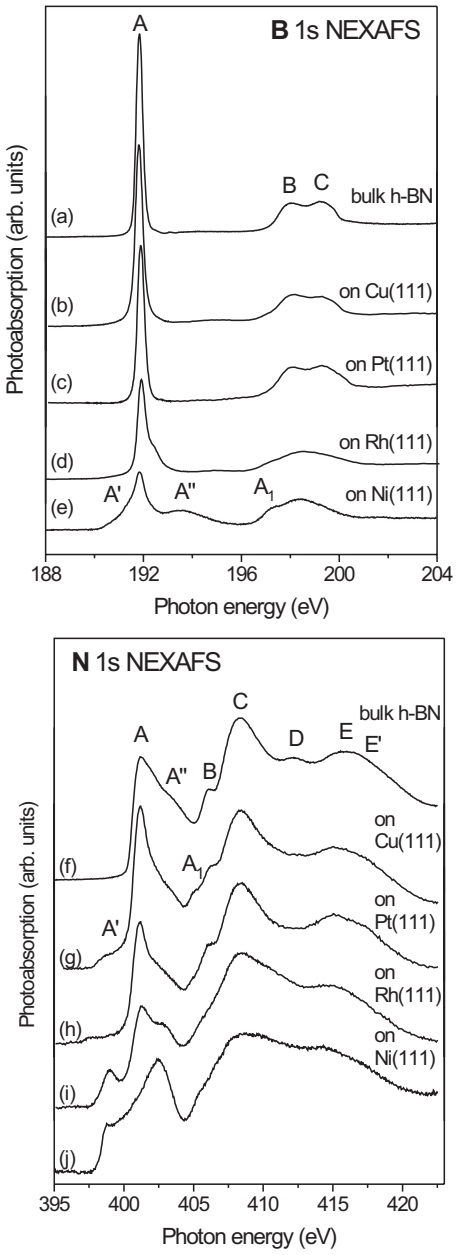

FIG. 4. Comparison of the B 1*s* and N 1*s* NEXAFS in different lattice-matched and lattice-mismatched interfaces and in the bulk *h*-BN. For all curves, $\Theta = 50°$.

tion. For both B 1*s* and N 1*s* NEXAFS, the changes in the spectra are most pronounced for the case of Ni(111) substrate. In contrast, the spectra of *h*-BN on Cu(111) and Pt(111) are very similar to those of bulk *h*-BN, with the obvious exception of shoulder A' appearing in the N 1*s* NEXAFS spectra. For *h*-BN on Rh(111), the shape of the B 1*s* and N 1*s* NEXAFS spectra is somewhat intermediate, implying that covalent d-π hybridization at the interface is significant but less pronounced than on Ni(111). Moreover, the N 1*s* NEXAFS shape [Fig. 4(i)] can be naturally divided into two overlapping profiles: one similar to the N 1*s* spectrum in bulk *h*-BN (with the characteristic π resonances A and A'') and another one resulting from the substrate-adsorbate chemical interaction (with peak A'). Thus, it is indicative of two essentially different chemical states for *h*-BN on Rh(111), in agreement with the STM results. In B 1*s* NEXAFS [Fig. 4(d)], the situation is similar, so that it is mainly the weakly bonded (elevated) *h*-BN building blocks which contribute to the sharpness of the π resonance A, while the strongly bonded (directly contacting the substrate) *h*-BN atoms contribute to the tails of this peak and to the changes in the σ-related structures B and C. Therefore, from Fig. 4, we conclude that the covalent bonding between *h*-BN and Pt(111) is weak, while on Rh(111), *h*-BN forms both

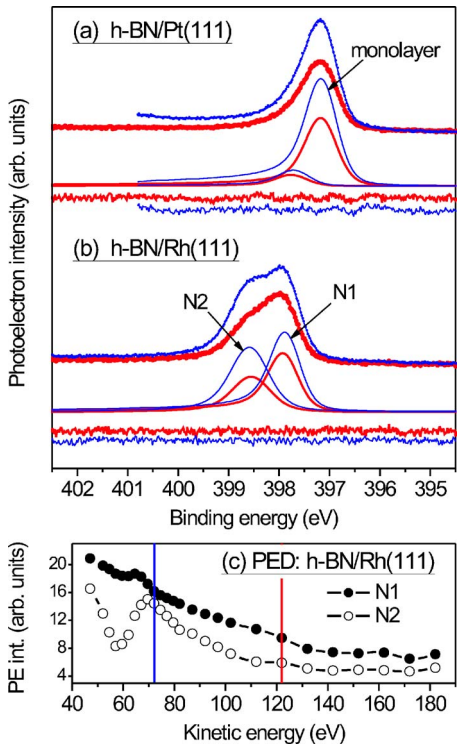

FIG. 5. (Color online) N 1*s* PE spectra from *h*-BN overlayers on (a) Pt(111) and (b) Rh(111) with the results of the corresponding peak fit analysis. Photon energy $h\nu$=520 eV for thicker (red) curves and 470 eV for thinner (blue) curves. (c) Intensity evolution for the two components of the N 1*s* signal measured in the normal emission mode from *h*-BN/Rh(111) as a function of kinetic energy. Kinetic energies used in (b) are indicated by vertical lines.

strongly and weakly bonded species (i.e., low-lying and elevated parts of the nanomesh, respectively).

C. Photoelectron spectroscopy

Core-level x-ray photoelectron spectroscopy (XPS) provides further confirmation of a nanomesh structure of *h*-BN on Rh(111) and its flat-monolayer structure on Pt(111). This can be observed clearly in the N 1*s* XPS signals, as shown in Fig. 5. Thicker (red) spectral curves correspond to more bulk-sensitive photoelectrons ($h\nu$=520 eV), and thinner (blue) curves are taken with more surface-sensitive conditions ($h\nu$=470 eV). Evidently, upon adsorption on Pt(111), the spectrum is dominated by just one strong component with the binding energy (E_B) of 397.18±0.05 eV relative to the Fermi level. The second weak component can result from a weak corrugation of the *h*-BN monolayer across the supercell. The overall spectral shape does not change in going from bulk-to surface-sensitive situation, thus confirming again the formation of just one atomic *h*-BN layer on Pt(111). On Rh(111), the spectrum is clearly different being composed of two components N1 and N2 with E_B =397.90±0.05 and 398.58±0.05 eV, respectively. The double-peak structure of the spectrum provides a confirmation of the coexistence of two types of *h*-BN species on Rh(111). The intensity ratio between the high-E_B and the low-E_B components varies with increasing kinetic energy of the photoelectrons, as illustrated for two different photon energies in Fig. 5(b). The effects of photoelectron diffraction (PED) considerably contribute to these variations. Therefore, the standard arguments of different surface sensitivity for different kinetic energies cannot be used here directly for assigning the photoemission (PE) signals to "upper" and "lower" parts of the nanomesh. Instead, we should analyze the PED curves obtained by systematic numerical fit of the N 1*s* signal measured at different photon energies [Fig. 5(c)]. Evidently, the intensity evolution is much more monotonous for the low-energy component (N1) than for the high-energy component (N2), reflecting mainly a decrease in the N 1*s* cross section. In contrast, component N2 has a sharp and strong (by a factor of 2) intensity oscillation between 50 and 80 eV, which is characteristic for a pronounced PED influence. Therefore, it is reasonable to conclude that signal N1 results from the outermost (elevated) sites of the nanomesh, while N2 is a signature of the sites in intimate contact with the substrate, because the latter is more sensitive to the backscattering by the substrate atoms and to the multiple forward scattering by the elevated *h*-BN sites. Another argument in favor of this interpretation is the position of the N 1*s* signal in the case of *h*-BN monolayer strongly chemisorbed on Ni(111), E_B=398.65 eV,[7] which is very close to the position of component N2, thus confirming a chemisorptive nature of this component. Here it is also worth mentioning molecular adsorption of N_2 on Ni(100), because in this case, the N 1*s* binding energy is also higher for the N atom contacting Ni directly than for the outer N atom.[10,11] Thus, we tentatively associate the low-E_B component N1 with the outer (physisorbed) parts of the nanomesh and high-E_B component N2 with the inner (chemisorbed) parts. The B 1*s* XPS signals from *h*-BN on Pt and Rh (not shown) are also composed of one and two peaks, respectively. However, in case of the nanomesh, the energy separation between the two B 1*s* peaks is smaller (about 0.42 eV) than between N 1*s* peaks (about 0.7 eV), making the assignment somewhat more ambiguous. Smaller mutual separation between the B 1*s* components may be interpreted as a smaller difference in the chemical state of the B atoms at the attracted and elevated sites of the nanomesh as a consequence of possible indirect (via N) bonding of boron to the substrate. On the other hand, different screenings of the core hole can be equally important. The B 1*s* binding energies are 190.67±0.05 and 190.25±0.05 eV on Rh(111) and 189.58±0.05 on Pt(111). It should be noted that N 1*s* and B 1 s binding energies for *h*-BN/Pt(111) are close to the values previously reported by Nagashima *et al.*: 397.3 eV for N 1*s* and 189.7 eV for B 1*s*.[3]

The strength of the orbital TM *d*–*h*-BN π hybridization at the *h*-BN/TM interfaces can be estimated by analyzing their valence-band photoemission (VB PE) spectra. In Fig. 6, we compare angle-integrated VB PE spectra of clean and *h*-BN covered Pt(111) and Rh(111) surfaces with the previously reported spectra of *h*-BN/Ni(111) and bulk *h*-BN.[7] All spectra are measured with the photon energy of 100 eV in normal emission, with the angle of 50° between the surface normal and polarization vector of the incident light. The bulk *h*-BN spectrum is arbitrarily shifted by 1.5 eV to lower E_B in order to facilitate comparison with the spectrum of the *h*-BN/Rh

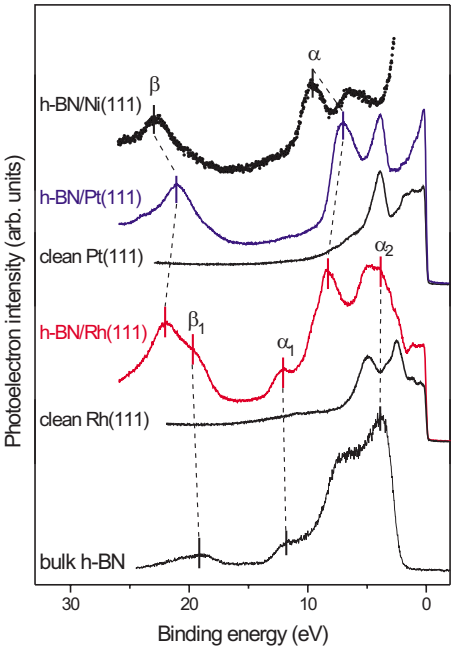

FIG. 6. (Color online) Valence-band PE spectra excited with $h\nu=100$ eV and $\Theta=50°$ and recorded in normal emission from several *h*-BN/TM interfaces and bulk *h*-BN. Note that features α and β correspond to *h*-BN monolayer in contact with the substrate, while features β_1, α_1, and α_2 are due to the elevated parts of the *h*-BN nanomesh on Rh(111).

interface. This shift results probably from the difference in the work-function values. It should be noted that the TM *d*-related features within 2 eV below the Fermi level are very sensitive to the substrate flatness and could vary in intensity depending on the preparation, while other spectral features are well reproducible.

As can be seen in Fig. 6, the main *h*-BN-related density of states (DOS) features in the VB PE spectra are α (composed mainly of the π band close to the Γ point[3,12]) and β (mainly N $2s$ DOS, sometimes called *s*-band for bulk *h*-BN[13]). The states corresponding to feature β lie too deep to participate significantly in the substrate-adsorbate bonding. Therefore, the variations in E_B of this feature in going from one interface to another reflect only variations in the work function, since E_B is measured relative to the Fermi level. Indeed, for physisorbed *h*-BN monolayers (such as on Pt or Pd), these nonbonding states should reference their binding energy rather to the vacuum level.[3] The position of feature α is influenced both by the work function variations and by the orbital TM *d*–BN π hybridization, because the π band can participate in the interface bonding. The energy difference $\Delta E=E_\beta-E_\alpha$ is 13.3 eV for *h*-BN/Ni(111), 14.1 eV for *h*-BN/Pt(111), and 13.7 eV for *h*-BN/Rh(111). As argued above, the orbital mixing at the *h*-BN/Pt(111) is very week, and the corresponding value of ΔE (14.1 eV) may be considered as the value for an isolated *h*-BN monolayer. On Ni(111), ΔE is reduced by 0.8 eV, in good agreement with the 1 eV shift of the *h*-BN π band on Ni(111) compared to Pt(111), as observed in the angle-resolved ultraviolet photoemission spectroscopy study by Nagashima *et al.*[3] For our consideration, the most important result is a substantial (by 0.4 eV) reduction in the ΔE value in going from the Pt(111) to the Rh(111) substrate, which reflects a considerable downward shift of the *h*-BN π band as a result of considerable orbital mixing at the *h*-BN/Rh(111) interface. This fact independently confirms the above conclusions based on the NEXAFS data. The analysis of the ΔE variations also allows us to conclude that *h*-BN on Rh(111) is chemisorbed somewhat weaker than on Ni(111) but considerably stronger than on Pt(111).

The spectra in Fig. 6 provide also one more compelling evidence for the nanomesh structure of *h*-BN overlayers on Rh(111). The spectrum from the *h*-BN/Rh interface has features α_1, α_2, and β_1, which are absent in the spectra of *h*-BN on Ni and Pt. These additional features clearly correlate in energy with the features of the VB PE spectrum in bulk *h*-BN, as long as this spectrum is shifted by 1.5 eV to lower binding energies, as mentioned above. Thus, features α and β in the VB PE spectrum from *h*-BN on Rh(111) are due to the *h*-BN species contacting the substrate directly, while α_1, α_2, and β_1 are signatures of the elevated sites of the nanomesh, which do not form covalent bonds with the substrate.

IV. DISCUSSION

The difference in the way *h*-BN interacts chemically (i.e., by forming covalent bonds) with Pt(111) and Rh(111) is caused mainly by two factors: (i) differences in the orbital overlap between *h*-BN $2s,p$ and TM nd, $(n+1)s$, and $(n+1)p$ $(n=4,5)$ states and (ii) differences in the *d*-band occupation between Pt and Rh. It should be noted that these two factors are not independent, since differences in the occupation also affect radial distribution functions and, as a consequence, the orbital overlap. In going from $4d$ to $5d$ elements, relativistic effects become significant, resulting in contracting the $6s$ orbitals and expanding the $5d$ orbitals.[14,15] Possibly, the overlap of the *h*-BN $2s,p$ states with more diffuse $5d$ orbitals is worse than with more contracted $4d$ orbitals. Another possible reason for the reduced orbital overlap is the increase in lattice mismatch between *h*-BN and the substrate in going from Rh(111) to Pt(111). The effect of the *d*-band occupation can also be important for the interface bonding. The electronic configuration changes from s^1d^8 to s^1d^9 in going from Rh to Pt. The additional *d* electron will reside in the states, which may be slightly antibonding relative to the interaction between substrate and *h*-BN overlayers, with the obvious consequence of weakening interfacial bonds.

At this point, a few words about the nature of chemical bonding are essential. In the borazine molecule (point group symmetry D_{3h}), both highest occupied molecular orbital and lowest unoccupied molecular orbital are of π type ($1e''$ and $2e''$, respectively).[16,17] Since the B_3N_3 ring is a building block of the *h*-BN sheets, the highest occupied and lowest unoccupied electronic states in bulk *h*-BN are bands of π symmetry (π and π^*, respectively) derived from the $1e''$ and $2e''$ molecular orbitals. On TM surfaces, these bands may mix with the nd, $(n+1)p$, and $(n+1)s$ states of the TM atoms $(n=3,4,5)$. If the *d* states are filled, the interaction is rather

weak, being mainly due to the *s* electrons. A good example is *h*-BN on Cu(111).[8] If the *d* states are partly unoccupied, they lie at the Fermi level and can mix with both π and π^* states of *h*-BN. This mixing leads to two kinds of charge transfer: from filled *h*-BN states into empty TM *d* states (π donating) and from filled TM *d* states into empty *h*-BN π^* states (π^* accepting or π^* back donating). The strength of covalent bonding at the interface is determined by the amount of this charge transfer, which, in its turn, is determined by the orbital overlap, as discussed above.

Let us now consider how the difference in chemical bonding may affect the formation of the *h*-BN nanomesh. In the extreme case of a very weak (vanishing) interaction between *h*-BN and a substrate, the exact location of the overlayer atoms relative to the substrate atoms is hardly important. The stronger the hybridization, the stronger the interfacial bonding and the larger the energy difference between favorable and unfavorable adsorption sites. This difference can be quite significant at *h*-BN/TM interfaces with strong chemical bonding. For example, at the lattice-matched *h*-BN/Ni(111) interface, the adsorption energy per unit surface cell calculated within the local-density-approximation–density-functional-theory (DFT) approach is close to 430 meV for the atomic configuration with N on top of Ni, and only about 140 meV for the less favorable configuration with B on top of Ni.[18] In the earlier generalized-gradient-approximation–DFT study of the same system by Grad *et al.*, no bonding at all could be reproduced for the B atop site occupation.[12] As soon as a lattice mismatch is introduced into the system, the *h*-BN monolayer becomes laterally strained, because *h*-BN atoms try to stay only in the favorable adsorption sites [e.g., N atop sites, like in the case of *h*-BN/Ni(111) (Refs. 4, 12, and 18)] but they cannot, due to the strong lateral sp^2 bonding within the *h*-BN sheet. Thus, contrary to the case of molecular adsorption, *h*-BN atoms have to reside on both favorable and unfavorable adsorption sites. This issue is illustrated in Fig. 7(a) showing a coincidence lattice resulting in a characteristic moiré pattern. Black circles are substrate atoms, and gray circles are N atoms (B atoms are omitted for simplicity). The supercell is indicated. This particular interface has the *h*-BN-to-metal cell ratio of 13:12 typical for the Rh(111) substrate, but the exact value of this ratio is not important for further consideration. The whole variety of nitrogen (boron) adsorption sites can be classified in four groups: toplike, bridgelike, hcp hollowlike, and fcc hollowlike (if a second-layer metal atom lies below the threefold hollow site, it is denoted as hcp hollow; otherwise, fcc hollow). Above the most favorable adsorption site, the *h*-BN monolayer has a tendency to approach the substrate surface forming covalent bonds and anchoring the monolayer to the substrate chemically [see Fig. 7(b)]. Upon increase in the strength of interfacial interaction, the area of these chemisorption sites increases. As a consequence, the monolayer becomes strongly corrugated and consists of physisorbed (elevated) sites and chemisorbed (attracted to the surface) sites [Fig. 7(c)]. The latter form apertures of the nanomesh. Some additional corrugation can exist due to the difference in adsorption energy between hcp and fcc hollow sites, because on TM (111) faces, the occupied *d* orbitals (t_{2g} in the O_h group representation) are directed toward fcc hollow sites,

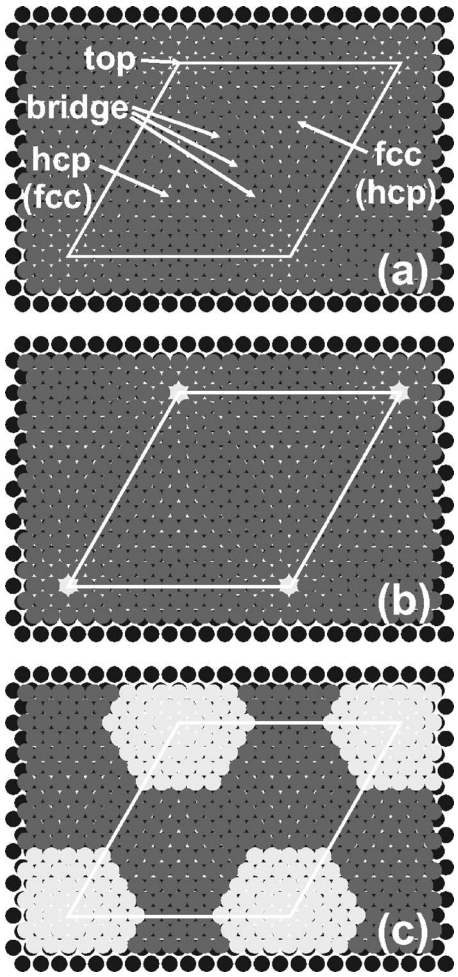

FIG. 7. A model 12:13 coincidence lattice with the characteristic moiré pattern; black circles are substrate atoms, dark (light) gray circles are physisorbed (chemisorbed) nitrogen atoms of an *h*-BN overlayer (boron atoms are omitted), and rhombus indicates the supercell. Possible adsorption sites within the supercell are shown in (a), formation of a single covalent bond (chemisorption) at a most favorable adsorption site upon increase of interfacial interaction is shown in (b), and formation of a chemisorption-mediated aperture within the supercell upon further increase of interfacial interaction is shown in (c).

while partly unoccupied *d* orbitals (e_g)—toward hcp hollow sites. This scenario correlates with the recent theoretical model proposed by Laskowski *et al.* for *h*-BN/Rh(111).[9] Thus, we believe that the difference in overlayer morphology between *h*-BN/Pt(111) and *h*-BN/Rh(111) is quantitative rather than qualitative: in both cases, *h*-BN forms a monolayer, but on Pt(111), it is relatively flat while on Rh(111) it is strongly corrugated. The main reason for the difference is a different strength of chemisorption at these interfaces.

It should be noted that there is no direct contradiction between our data and the original double-layer model of the nanomesh;[6] therefore, this model cannot be excluded based on the presented spectra. On the other hand, the single-layer model of the nanomesh allows us to explain differences in the spectra between *h*-BN/Pt(111) and *h*-BN/Rh(111) in a more evolutionary way, without a necessity to assume a sud-

den formation of big regular holes in the *h*-BN monolayer (and, consequently, a lot of broken lateral bonds) in going from platinum to rhodium. For extracting more accurate structural information about the *h*-BN morphology on the TM surfaces, more similar systems should be characterized spectroscopically in order to link the spectral evolution with the strength of interface bonding. This work is now in progress for the *h*-BN/Ir(111) and *h*-BN/Ru(0001) interfaces.

V. CONCLUSIONS

By a combination of several experimental techniques, we have demonstrated that a considerable structural difference does exist between *h*-BN overlayers formed on Pt(111) and Rh(111) despite the same symmetry and close lattice parameters of these TM substrates. On Pt(111), *h*-BN forms a rather flat single monolayer, while on Rh(111), it grows in a nanomesh form, as originally observed by Corso *et al.*[6] We attribute this difference to the peculiarities of the interfacial chemical bonding. On Pt(111), *h*-BN is bonded weakly because of the weak Pt d,s–*h*-BN π orbital mixing, while on Rh(111), the bonding is significantly stronger as a consequence of better orbital overlap. We suggest that stronger *h*-BN chemisorption on Rh(111) results in a much stronger corrugation of the adsorbed monolayer due to larger difference in energy between favorable and unfavorable adsorption sites within the interfacial supercell. On the whole, our study shows that the details of the interfacial chemical bonding are essential for understanding the underlying mechanism of the *h*-BN nanomesh formation.

ACKNOWLEDGMENTS

This work was financed by the Swedish Foundation for Strategic Research, the Swedish Research Council, the Crafoord Foundation, the Knut and Alice Wallenberg Foundation, and the Russian Foundation for Basic Research (Project No. 06-02-16998). A.S.V. gratefully acknowledges the support of Uppsala University and MAX-lab.

*Electronic address: alexeip@maxlab.lu.se

[1] M. T. Paffet, R. J. Simonson, P. Papin, and R. T. Paine, Surf. Sci. **232**, 286 (1990).
[2] A. Nagashima, N. Tejima, Y. Gamou, T. Kawai, and C. Oshima, Phys. Rev. B **51**, 4606 (1995).
[3] A. Nagashima, N. Tejima, Y. Gamou, T. Kawai, and C. Oshima, Phys. Rev. Lett. **75**, 3918 (1995).
[4] E. Rokuta, Y. Hasegawa, K. Suzuki, Y. Gamou, C. Oshima, and A. Nagashima, Phys. Rev. Lett. **79**, 4609 (1997).
[5] C. Oshima and A. Nagashima, J. Phys.: Condens. Matter **9**, 1 (1997).
[6] M. Corso, W. Auwärter, M. Muntwiler, A. Tamai, T. Greber, and J. Osterwalder, Science **303**, 217 (2004).
[7] A. B. Preobrajenski, A. S. Vinogradov, and N. Mårtensson, Phys. Rev. B **70**, 165404 (2004).
[8] A. B. Preobrajenski, A. S. Vinogradov, and N. Mårtensson, Surf. Sci. **582**, 21 (2005).
[9] R. Laskowski, P. Blaha, T. Gallauner, and K. Schwarz, Phys. Rev. Lett. **98**, 106802 (2007).
[10] W. F. Egelhoff, Surf. Sci. **141**, L324 (1984).
[11] A. Nilsson, H. Tillborg, and N. Mårtensson, Phys. Rev. Lett. **67**, 1015 (1991).
[12] G. B. Grad, P. Blaha, K. Schwarz, W. Auwärter, and T. Greber, Phys. Rev. B **68**, 085404 (2003).
[13] E. Tegeler, N. Kosuch, G. Wiech, and A. Faessler, Phys. Status Solidi B **91**, 223 (1979).
[14] D. M. P. Mingos, *Essential Trends in Inorganic Chemistry* (Oxford University Press, Oxford, 1998).
[15] G. C. Bond, Platinum Met. Rev. **44**, 146 (2000).
[16] W. P. Anderson, W. D. Edwards, M. C. Zerner, and S. Canuto, Chem. Phys. Lett. **88**, 185 (1982).
[17] J. P. Doering, A. Gedanken, A. P. Hitchcock, P. Fisher, J. Moore, J. K. Olthoff, J. Tossell, K. Raghavachari, and M. B. Robin, J. Am. Chem. Soc. **108**, 3602 (1986).
[18] M. N. Huda and L. Kleinman, Phys. Rev. B **74**, 075418 (2006).